TITLE: EPR of Site-Directed Spin-Labeled Proteins: A Powerful Tool to Study Structural Flexibility

AUTHOR: Inés García-Rubio

ADDRESS: Centro Universitario de la Defensa. Ctra de Huesca s/n, 50090 Zaragoza

inesgr@unizar.es

Abstract

Electron Paramagnetic Resonance is a spectroscopic technique which, in combination with site-directed spin-labeling, provides structural and dynamic information about proteins in conditions similar to those of their physiological environment. The information is sequence-resolved as it is based on probing the local dynamics of a paramagnetic label incorporated as a side chain of a selected amino acid. This technique does not impose a limit on the size of the protein or protein complex, as long as it is amenable to site-directed mutagenesis. Reliable distance distributions between two or more labels (identical or different) can also be obtained. The mean value, width and shape of distance distributions, as well as their dependence upon the state of the protein or interactions with physiological partners, provides insight into order-disorder transitions and the roles of protein flexibility.

The main potentialities of the technique are revised and illustrated with examples of proteins for which order-disorder play an important role.

Keywords: Site-Directed Spin-Labeling; order-disorder transition; protein flexibility; Electron Paramagnetic Resonance; Intrinsically Disordered Protein; structural disorder

Introduction

The traditional view on protein structure, in which the structure of a protein is determined by the amino acid sequence with a unique conformation of minimum free energy, is being challenged, as more and more examples are found for which not only there is no single structural conformation, but rather flexibility and conformational disorder. This is the case of the so-called intrinsically disorderd proteins (IDP), the most recently discovered type of proteins, characterized by a lack of well-folded, fixed and ordered three-dimensional structure. IDPs can sample a heterogeneous assembly of conformations ranging from fully unstructured to partially structured and include random coils, pre-molten globules or structured domains linked by an intrinsically disordered domain (IDD) [1, 2]. Moreover, there is increasing evidence that flexibility is of central importance to the function of many proteins, in particular, it is essential to key functions where molecular recognition plays an important role such as regulation, molecular assembly, signaling or molecular recognition [3-5].

Con formato: Color de fuente: Automático

Código de campo cambiado

Con formato: Color de fuente: Automático

Código de campo cambiado

Con formato: Color de fuente: Automático

In this context, the aim is to describe the modes and amplitudes of conformational flexibility and characterize their time scales in physiological conditions. However, there is only a limited number of experimental techniques suited for investigation of IDPs. Hence, there is a need for spectroscopic tools that are able to address these challenges. As already evidenced in previous literature [6-8], Electron Paramagnetic Resonance (EPR) combined with Site-Directed Spin Labeling (SDSL-EPR) is one of them, since it is able to probe the dynamics of the protein with residue resolution, and therefore describe flexibility along the polypeptide chain. The availability of distance distributions between selected points in the sequence further contributes to characterize order- disorder transitions and interaction sites in protein-protein interactions [9, 10]. Further integration of this information with that provided by or other sources in a conformational model will address the question of whether the protein explores the whole possible range of conformations, or has restricted flexibility, and, if so, how much [11, 12].

In this review, the main potentialities of EPR will be illustrated using examples from the literature on EPR studies of spin-labeled Intrinsically Disordered Proteins (IDPs), on proteins visiting a disordered state, or on those having a flexible domain.

Spin Labeling

Since most of the IDPs, as many other biological macromolecules, are not paramagnetic, the introduction of a paramagnetic probe is needed in order to extract relevant information about the protein by EPR. This procedure is called spin labeling. A spin label is a paramagnetic moiety whose EPR spectrum is able to provide information about the molecule it is attached to. On one hand the label might constitute in some cases a perturbation to the protein molecule, but on the other hand it brings specificity, as the probe is most often the only signal in the EPR spectrum. In fact, spin-label EPR studies are not limited by the size of the protein, its solubility or the presence of other partners or macromolecules, so it is possible to perform EPR experiments in crowded environments like biological membranes or even cells.

Moreover, given that paramagnetic labels report on properties of the local environment (normally dynamics, polarity or distance constraints), one can ideally select the position of interest, or even scan through the protein sequence looking for changes along the protein chain. This is the idea behind the technique *site-directed spin-labeling* introduced by the group of W.L. Hubbell about 30 years ago [13, 14]

Nitroxide Spin Labels

In order to make a wise choice when aiming to study dynamics of a protein, one has to bear in mind that the most important properties of a spin label are stability and anisotropy. On one hand, the label should have a stable paramagnetic moiety, which yields an EPR signal in the range of temperatures relevant for the study, i.e. close to room temperature. On the other hand, its spectrum must be sensitive to the dynamics of the protein towards reorientation, which is related to the anisotropy of the spectrum. Additionally, the label should incorporate a reactive group able to selectively react with a particular amino acid in the protein sequence

without disturbing its native fold. Because they nicely fulfill the aforementioned conditions, most widely used spin labels for EPR studies on proteins in general are based on nitroxide radicals. In particular, this applies to IDPs.

Nitroxides are heterocyclic free radicals carrying an unpaired electron (S = ½) in a N-O· bond. The nitrogen atom has a 99.6% natural abundance of isotope ^{14}N, which has nuclear spin I = 1. Bulky substituents on the carbons attached to the nitrogen (normally methyl groups, see Fig. 1) sterically shield the radical and confer the desired stability *in vitro*. Under reducing conditions, such as the ones found *in vivo*, nitroxides are no longer stable, but it has been shown that five-membered ring nitroxides (e.g. PROXYL) are more stable than six-membered rings (e.g. TEMPO) [15]. Also, it has been reported that bulkier substituents like gem-diethyl can slow down the process in these conditions and the radical remains up to a few hours before being reduced [16-18]. The EPR active part of the label is attached to a short tether and functionalized with a chemical group able to react with the side chain of an amino acid, most commonly cysteine.

Spin Labeling of Cysteine Residues

By far, the most common label for EPR applications in proteins is the (1-oxyl-2,2,5,5-tetramethylpyrroline-3-methyl) methanethiosulfonate (MTSSL). This is due to the specificity for the sulfhydryl group of cysteine with which MTSSL reacts to form a disulfide bridge. The resulting side group is commonly identified as R1 and has a small molecular volume, close to the one of a tryptophan side chain. The disulfide bridge can be broken and the label released in the presence of dithiothreitol (DTT) or other reducing agents. The linker between the nitroxide ring and the protein backbone makes the R1 side chain flexible and therefore perturbation of the native structure is commonly minor. This flexibility, caused mainly by fluctuation of dihedral angles χ_4 and χ_5 (see Fig. 1.B) results in the electron spin sampling different positions in space depending on the conformational distribution of the linker [19].

Other bulkier spin labels are functionalized with maleimide (4-maleimide-TEMPO, MSL), a group that reacts irreversibly with cysteine to form a thio-ether bond. Acetamide-functionalized spin labels, such as 3-(2-Iodoacetamide)-2,2,5,5-tetramethyl-1-pyrrolidinyloxy (IAP), also react with cysteine via a C-S bond. Both alternatives are used when reducing conditions are required for protein preparation [20, 21].

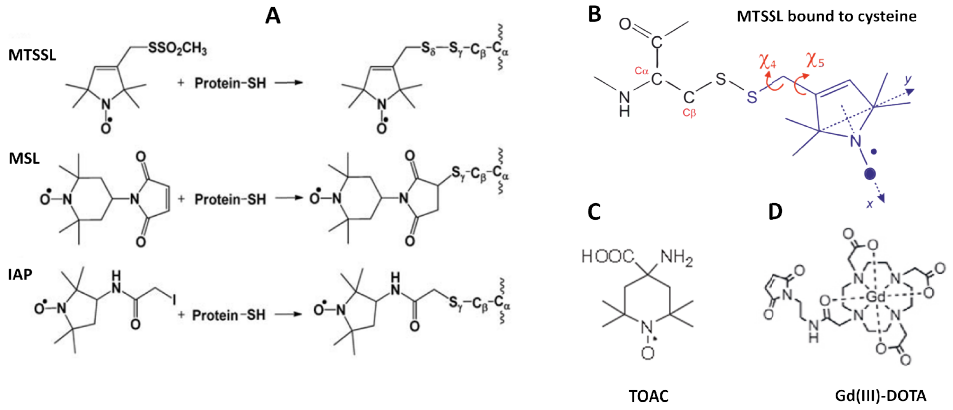

Figure 1. Spin labels. **A**. Methanethiosulfonate spin label (MTSSL), Maleimide-TEMPO (MSL) and iodoacetamide-proxyl (IAP) and their reactions with the Cysteine side chain. **B**. MTSSL bound to a cysteine backbone, the most flexible bonds are labeled χ_4 and χ_5. The orientation of the gyromagnetic and hyperfine axes is indicated on the NO· moiety with dotted axes. **C**. Chemical structure of TOAC spin label. **D.** Chemical structure of maleimide- Gd(III)-DOTA spin label.

The spin labels mentioned above are commercially available from different chemical providers. In order to perform site-directed spin labeling, one or several cysteine residues must be engineered at the sites of interest, usually by site-directed mutagenesis. Obviously, known important residues in terms of function or structure should not be labeled. For folded proteins, Cys, Ile, Leu, Met, Ser, Thr and Val are considered favorable labeling sites as they are non-coordinating, uncharged, hydrophobic groups, whereas Gly and Pro mutation should be avoided due to their different preferences for backbone dihedral angles, as well as aromatic residues that might be involved in π interactions [19]. For IDPs all this might be irrelevant, as there is no protein structure to be altered; however, since many of them are involved in molecular recognition and they do fold, maybe only partially, into a structure upon binding of molecular partners, when possible, it might be wise to follow these recommendations for IDPs as well.

In order to avoid spurious labeling, if there are native cysteine amino acids in the protein sequence, they must be substituted, usually by serine or alanine. Once the designed mutant has been produced and purified, it is often convenient to incubate it with DTT 2-10 mM for about an hour in order to reduce the disulfide bonds that might have formed during the process. The protein concentration is advised to be in the 10-30 µM range for this procedure. Immediately after careful removal of DTT (max 1 µM residual concentration) the samples are incubated with a, typically, 10 fold molar excess of spin label for several hours at room temperature or 4 ˚C, depending on the stability of the protein. One has to be careful not to exceed a concentration of MTSSL above 500 µM, as spin biradicals can form and the spin label would not be available for reacting with the protein [22]. For IDPs all of the residues are expected to be accessible to the solvent and therefore readily labeled even after a few minutes of incubation. Excess of free label has to be thoroughly eliminated by dialysis,

desalting chromatography or centrifugal filtering procedures. The last step would be to concentrate the sample for the experiment.

For X-band measurements, very good signal-to-noise ratios are obtained for samples around 100 µM spin label concentration, however, it is possible to measure samples down to 1 µM of spin labeled proteins in 20 µl volume samples. The spin labeling efficiency is the ratio between the spin concentration and the protein concentration quantified independently, typically by spectroscopic methods. Spin quantification for assessing the success of the labeling operation can be done by comparing the double integral of the background-free continuous-wave (CW) EPR spectrum with the one of a nitroxide standard of known concentration measured at exactly the same experimental conditions. Mass spectrometry can also be used to quantify the spin labeling efficiency [23]. Labeling efficiencies per site in the 80-100% range are considered good. Efficiencies above 100% can be an indication of undesired effects like non specific labeling, the presence of an impurity containing cysteines, or even residual free label in the solution. It is important to note that, as we will discuss later, the CW-EPR spectrum of spin labeled IDPs is a set of three symmetric and sharp lines, and so is the spectrum of free label; therefore it is not always obvious to recognize from the spectrum when there is a small amount of free label in the sample. In order to avoid misinterpretations of the spectra due to contamination with free label, the advice is to keep the last centrifugation flow-through upon sample preparation and measure it to check for the presence of label. In case the sample still contains free label, further washing is necessary.

Spin Labeling with no Involvement of Cysteine Residues

When the target protein has many native cysteines, or cysteines that play an important functional or structural role, addressing the spin label to the cysteines is not a good idea. Other spin labeling strategies aim at side chains of Tyrosine [24]. Labeling of lysines is possible since maleimide or acetamide react with amines at high pH [25, 26].

Alternatively, the insertion of genetically encoded unnatural amino acids that can be either subsequently spin labeled or directly biosynthesized from previously purified synthetic spin-labeled amino acids has been demonstrated to work [27, 28] yielding a longer and more flexible side chain than the native amino acid. Other nitroxide spin-labeling strategies include peptide synthesis introducing spin labeled artificial amino acids like 2,2,6,6-tetramethyl-piperidine-1-oxyl-4-amino-4-carboxylic acid (TOAC, see Fig. 1.C) as part of the sequence [29]. The direct bond of the nitroxide ring to the C^{α} makes the TOAC side chain very rigid [30], which can distort the protein structure [31]. Other artificial spin-labeled amino acids with restricted flexibility have been designed for peptide synthesis, which can be combined (semi-synthesis) with chemoselective methods to attach the spin labeled peptides to protein fragments produced by recombinant methods when trying to label large proteins [32].

Spin Labeling Beyond Nitroxides

Although nitroxides remain the spin labels of choice for measuring protein dynamics using CW-EPR, other spin labels are gaining increasing attention due to the development of pulsed EPR methods such as DEER (Double Electron-Electron Resonance) or RIDME (Relaxation Induced Dipolar Modulation Enhancement) used for distance determination between paramagnetic

centers [33]. Orthogonal labeling, that is, labeling different sites with different kind of probes, also requires the availability of spin labels with spectra different from the one of nitroxides [34, 35]. Lately, Gd(III) spin labels have attracted much interest for distance measurements in proteins [36-39]. The EPR properties of Gd(III) are very different from the ones of nitroxides; due to its high-spin character (S = 7/2) it has several spin transitions, and low temperatures are needed to observe the signal. Its central line narrows at higher fields as a consequence of the spectral anisotropy being caused by the zero-field energy term, with the consequent improvement of sensitivity at higher frequencies with respect to X-band, and, therefore,potentially amenable to measure longer distances [40]. Nowadays there are commercially available Gd(III) spin probes based on maleimide-DOTA (Tetraazacyclododecanetetraacetic acid) (see Fig. 1.D.) and maleimide-DTPA (Diethylenetriaminepentaacetic acid) . DEER methods are optimized for selective measurement of Gd(III)-Gd(III), Gd(III)-nitroxide or nitroxide-nitroxide distance distributions in the same sample [41, 42]. Finally, unlike nitroxides, Gd(III) complexes are stable in reducing environment and can be used for in-cell applications [43-47].

Cu(II) and Mn(II) complexated by quelators like EDTA or TETAC are also being considered for site-directed spin labeling of proteins, methods and protocols for Mn(II)-Mn(II), Cu(II)-Cu(II) and Cu(II)-nitroxide distance measurements have been established [48-52]. Triltyl radicals, having an extremely narrow EPR signal are being explored for orthogonal labeling of protein complexes in combination with nitroxides resulting in a selective determination of distance distributions [53], or for distance determination between labels at room temperature [54].

Whatever the label and the labeling strategy should be, after mutant production and spin labeling procedures, it should be checked that the incorporation of the spin label has no effect on the structure (or lack thereof) of the protein, nor the functionality. Control experiments to check the function and comparison of the labeled mutants with the native protein using other spectroscopies (UV-VIS, far UV-CD) can be routinely used for that.

CW-EPR Spectrum of Nitroxides

As mentioned above, in nitroxides the free radical resides in the N-O· bond, their g-values are not far from the free electron gyromagnetic ratio 2.0023. About 40% of the spin density is located at the nitrogen and 60% at the oxygen atom. The portion residing at the nitrogen atom is responsible for the magnetic interaction with the nuclear spin of nucleus ^{14}N , or hyperfine interaction. Since the electron spin resides mainly in a p_z orbital and this orbital lacks spherical symmetry but has an axial symmetry, the interaction is not isotropic but it has a very different value (larger) in the direction of p_z (molecular z axis). Also, the g-tensor is not exactly isotropic and has typical values of g_x = 2.0091-2.0088, g_y = 2.0059, g_z = 2.0027 [19, 22]. Both, the g-tensor axes and the hyperfine axes are aligned with the molecular axes: x, in the direction of the N-O bond, z in the direction perpendicular to the nitroxide ring and y in the direction perpendicular to the other two (see Fig. 1.B)

When the external magnetic field is oriented along the molecular *z*-axis of the nitroxide, its EPR signal will consist of three lines centered at the magnetic field corresponding to g_z,

$B(g_z) = \frac{h\nu}{\mu_B g_z}$, each one corresponding to one of the three possible values of the third component of the nuclear magnetic moment, I_z = +1, I_z = 0 and I_z = -1, split by the hyperfine interaction A_z (see Fig. 2.A). On the other hand, if the magnetic field is oriented along the N-O bond direction (*x*-axis), the EPR spectrum will be centered at g_x and the three lines split by the value A_x. For intermediate positions one would find intermediate positions of the center of the spectrum and the splitting, so that the spectrum of all orientations present in the sample sums up to the so-called "powder spectrum" shown in Fig. 2.A. In order to improve the s/n ratio, EPR spectrometers perform lock-in detection. This is technically achieved by adding a modulated contribution to external magnetic field, normally at 100 kHz. The modulation field is not strong (modulation amplitude 0,01 - 1 mT), but a consequence of this procedure is that the spectrum obtained experimentally has the shape of the first derivative of the absorption line with an intensity proportional to the modulation amplitude, when this amplitude amounts to less than the linewidth. Fig. 2.B (up) is the typical outcome of an experiment of an *immobilized* nitroxide at X-band frequencies (~ 9.5 GHz). For Q- and W-band (~ 34 and ~ 95 GHz respectively), the value of the anisotropic hyperfine coupling does not change, but the g-anisotropy scales up with the magnetic field so the spectra become more anisotropic and take on different characteristic shapes (see Fig. 2.B).

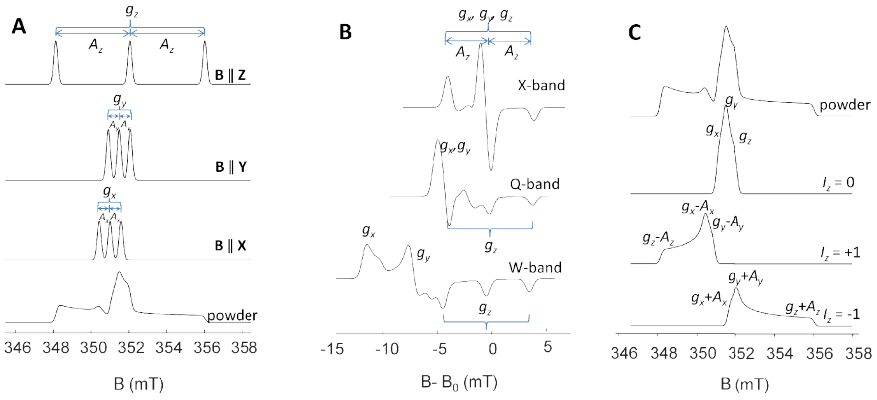

Figure 2. Spectra of nitroxides in the rigid limit. **A**. Simulated X-band absorption EPR spectra for particular orientations of the external magnetic field with respect to the axes of the nitroxide (single-crystal spectrum). Magnetic field oriented along z- (up), y- and x- molecular axes. At the bottom: powder spectrum corresponding to the sum of all equally likely possible orientations. **B**. Derivative powder EPR spectra of nitroxides at X-, Q- and W-band. The magnetic field axis is plotted relative to the one corresponding to g_z. **C**. Powder (all orientations) absorption EPR spectrum at X-band (top) and separated powder spectra of only the molecules with the indicated third components of the nuclear spin of ^{14}N. Note that although labels g_z, g_y or g_z appear in the spectra, they all refer to $B(g_z)$, $B(g_y)$ and $B(g_x)$. All simulations were performed using the function pepper of EasySpin.

The *share* of electron spin population between the oxygen and nitrogen atoms is influenced by the polarity of the environment. In apolar environments the electron spin density resides in the oxygen, while in polar solvents, the electron spin density is shifted towards the nitrogen atom increasing slightly the nitrogen hyperfine coupling. The outer splitting of the EPR

spectrum can vary from A_z = 3.3 mT in apolar environment to 3.7 mT in protic solvents [22]. Also the value of g_x varies with the polarity of the nitroxide environment in the range specified above; it decreases with increasing polarity [22], but this effect is only reliable when measured at high frequency experiments (W-band).

If we have a look at the powder or *rigid limit* spectrum we can examine it from a different point of view: all of the molecules in the spectrum are divided in three sets depending on its nuclear spin state I_z = +1, I_z = 0 and I_z = -1 (Fig. 2.C). Each of the three sets contains all possible orientations and their EPR spectra have the features referring to the orientations of the molecules with respect the magnetic field. Now, if the molecules are not static but rotating in the time scale of the experiment, the EPR spectrum will reflect that movement. The time scale of the molecular rotations is normally characterized by their rotational correlation time, τ_c. This parameter gives an idea of the time after which molecules with initially identical orientations lose their alignment [55]. In turn, the time scale of the EPR experiment is determined by the spectral anisotropy, that is, the maximum difference in the EPR line positions of molecules with different orientations.

Intuitively one can imagine that if the molecule is rotating extremely fast with respect to the time frame of the experiment any anisotropy will be averaged out and only the isotropic part of any interaction will be observed, the analogy can be made with a picture of a rotating object taken with a long exposure time, where only a blurry big dot would be captured. The EPR spectra in Fig. 2.C. of such a fast rotating object would collapse into one single line at the centroid of each spectrum, which is, for I_z = -1, at the magnetic field corresponding to g_{iso}, B(g_{iso}), plus the contribution of the hyperfine coupling A_{iso} in magnetic field units, at B(g_{iso}) for I_z = 0 and for I_z = +1 at B(g_{iso}) - A_{iso}. The result of such a measurement is a spectrum in the *isotropic limit*, three lines centered at the value corresponding to $g_{iso} = \frac{g_x+g_y+g_z}{3}$ and equally split by $A_{iso} = \frac{A_x+A_y+A_z}{3}$. Such an X-band EPR spectrum is found in nitroxides for values of τ_c shorter than 10 ps, see Fig. 3. Here, the linewidth is determined by unresolved hyperfine couplings. As the movement gets slower and the correlation time increases the lines get broader, especially the high-field line, which has a larger anisotropy (see Fig. 3). This is called the *fast tumbling* regime because the speed of rotation is fast in relation to the spectral broadening. Therefore, if the spectrum is more anisotropic, it will need a faster the rotation to collapse in a narrow line. If the rotation is further slowed down to a τ_c longer than 3 ns, the spectrum gets distorted (*slow tumbling* regime) and finally reaches the *rigid limit* for correlation times longer than 100 ns. This is when, according to our analogy, the snapshot of the camera is fast enough it can capture all the details of the object as if it were still.

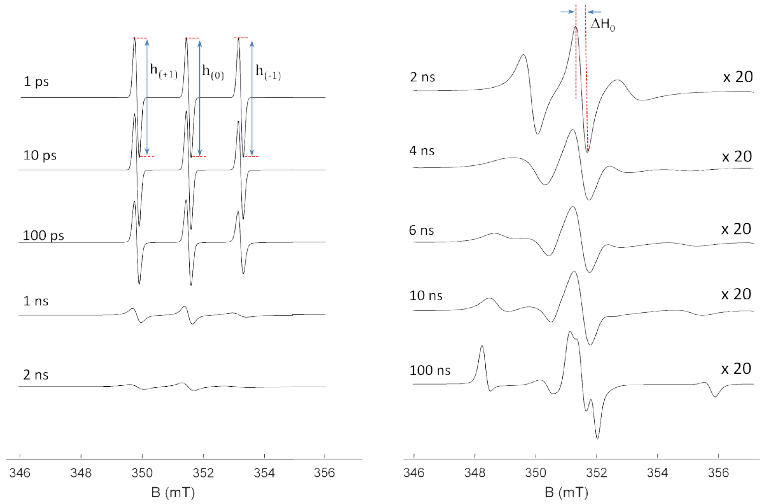

Figure 3. Dynamic range of the nitroxide spin probe. Simulated X-band EPR spectra of nitroxides undergoing isotropic reorientation. The correlation times, τ_c, are indicated in the figure. Although the double integral remains constant, note the intensity loss that takes place upon increasing τ_c, especially dramatic in the 0.1 – 2 ns range. The spectra in the right column are amplified by a factor of 20 with respect to the ones on the left. The first and last spectra correspond to the isotropic limit and to the rigid limit respectively. Some of the spectral parameters that have been used to characterize dynamics of nitroxide probes are defined: the intensities of the low-, mid-, and high-field lines, for fast dynamics; and the width of the central line for dynamics in the slow tumbling range. Simulated with EasySpin function chili using (g_x, g_y, g_z) = (2.0088, 2.0061, 2.0026), (A_x, A_y, A_z) = (5.8, 5.8, 39.5) mT and a Gaussian isotropic line width of 0.18 MHz.

Protein Dynamics

Nitroxides are appropriate probes for protein dynamics because their anisotropy allows exploring a time range during which biologically relevant motions take place. In Figure 3, simulations based in a rotational Brownian diffusion model, also known as isotropic rotation, are presented. For this model every molecular orientation is equally likely but since most of IDPs reported in the literature can be simulated using this model in the fast tumbling regime, it is a relevant example. Experimental spectra in the slow tumbling regime are extremely sensitive to the details of the motion [19, 56]. Actually, this motion can have contributions from different phenomena. 1) The overall rotation of the protein (global tumbling); if the protein is big enough or in 30% sucrose, this contribution is negligible [57, 58]. 2) The side-chain conformational dynamics. Many structural studies have been based on the mobility of R1 studied by EPR. Since it can report about dynamics of its local environment, the information can be translated to whether the probe is in a buried position of the structure, exposed to the solvent or in a tertiary contact site [59-61]. In principle if an IDP is in an unfolded state with no secondary or tertiary structure, one can assume that the side chain of the spin probe is

exposed to the solvent, with unrestricted configurational dynamics. 3) The backbone fluctuations [62], which the motion we are interested in when studying IDPs.

Reliable interpretation of the lineshapes of spectra in the slow tumbling regime can only be made with a dynamic model and the simulation of EPR spectra at multiple frequencies [63]. Also, given the protein structure as an input, successful simulation of the CW spectrum has been achieved by molecular dynamic simulations [64, 65]. Both approaches are difficult, so parameters have been defined to interpret the spectra semiquantitatively, such as the linewidth of the central line (ΔH_0 or δ, depending on the reference), the second moment of the spectrum $\langle H^2 \rangle$ [66], or the ratio h(+1)/h(0), see Fig. 3. The numerical values of these parameters increase as the frequency of the reorientational motion of the nitroxide is reduced. For IDPs, large, fast and probably close to random backbone fluctuations are expected which yield X-band spectra in the fast-motional regime. These spectra are much less dependent on the details of the nitroxide motion and are normally satisfactorily simulated using an isotropic model of motion with correlation times in the 0.1 - 3 ns range [20, 67-69]. For the interpretation of such CW spectra to be reliable, very careful collection of the data set is required. The temperature of the experiment depends on the stability of the protein, but it needs to be performed in liquid solution to allow for reorientation dynamics. Typically, either room temperature or 4 ˚C is used as a default. Some other times the experiments are recorded as a function of temperature to find interesting effects [7, 67]. The use of sucrose or glycerol is recommended to increase the viscosity of the solution and/or to reach temperatures in the liquid phase below the freezing point of water in order to slow down the overall tumbling of the protein [57]. For X-band measurements, about 20 µl of sample, even less if needed, are inserted in a glass capillary (0.5 mm inner diameter) and placed in the center of the resonator. Normally, a scan of the magnetic field of about 15 mT centered at the resonance position should cover the entire spectrum. If, as expected, the motion of the label is in the fast tumbling regime, the spectrum will have very sharp lines. In this case the one has to make sure the modulation amplitude is not producing distortions of the spectrum due to overmodulation. This parameter should be less than 0.15 mT for nitroxides. The power saturation curve should also be checked for the particular kind of sample and resonator to avoid distortions in the intensity and shape of the lines due to power saturation of the spectra.

In the fast motion regime observed in IDPs, faster dynamics mean narrower lines. Since the number of spins is proportional to the double integral of the spectrum, a faster rotational motion is translated into a higher intensity in the spectrum. This is the reason why some authors, in order to compare different spectra, present the spectra normalized to the same double-integral value, so that differences in intensities reveal differences in rotational dynamics in a very visual way [35, 67]. In Fig. 4 one of such normalized plots is shown to illustrate the comparison among the EPR spectrum that was done in [67] for different spin probes attached to the same protein site in IA_3, an IDP that inhibits yeast proteinase A. The spectra correspond to three different probes, MTSSL, MTL and IAP, bound to the cysteine of the mutant S14C. The intensities of the spectra normalized to the same second integral reveal subtle changes in the mobility that are to be expected in view of the length and flexibilities of the linkers (see Fig. 1). The maleimide probe is a bit longer that MTSSL but also bulkier due to the maleimide-TEMPO group so one can rationalize the smaller intensity in the spectrum with a more hindered rotation of the probe side chain. On the other hand, IAP has a longer tether

with respect to MTSSL which makes the motion of the probe slightly faster. Additionally, for every probe, the addition of increasing amounts of trifluoroethanol leads to smaller intensities and therefore to a slower dynamics, indicating the formation of an α-helical structure.

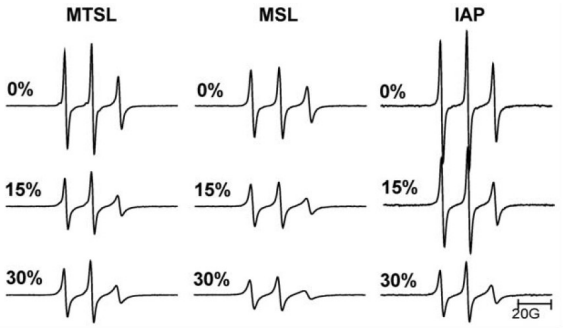

Figure 4. X-Band CW-EPR spectra of different nitroxide labels. The same variant, S14C, of the IDP protein IA3 was labeled with MTSSL (left), MSL (center) and IAP (right) in the presence of increasing concentrations of trifluoroethanol (TFE), a secondary structure stabilizer. The plots were normalized to the same area so that differences in intensity report directly on dynamics. Reproduced with permission from [67]

One of the main strengths of EPR in IDPs is that it can detect conformational changes in the protein when they involve changes in backbone flexibility. For the fast motional regime observed for IDPs, the most useful semiquantitative EPR spectral parameters to compare rotational dynamics are the ratio between the low and center field lines, *h(+1)/h(0)* [7], or the percent variation of the intensity of the high-field line *h(-1)* [67]. However, most of the examples found in the recent literature express mobility results using the correlation time τ_c obtained from simulations of the spectrum based on isotropic motion models. Several possibilities are openly available for simulations of dynamic EPR spectra. One of the most popular in the EPR community is EasySpin, a MATLAB toolbox for simulating and fitting a wide variety of EPR spectra [70]. It is downloadable from the website www.easyspin.org, where detailed documentation of the different functions and many examples can be found. The download is free of charge but it needs to run in the MATLAB environment, which requires a license from the Mathworks co. Among other EPR utilities, simulations of EPR spectra in the fast-motional regime following the Redfield theory are implemented in the function *garlic* and Liouville Stochastic equation simulation methods are implemented in the function *chili* [55]. Although the simulation tool allows for more sophisticated dynamic simulations, all of the recent literature that was looked up on EPR of IDPs seems to fit satisfactorily their spectra with a simple isotropic motion model, which is in agreement with very fast and unrestricted backbone fluctuations. SimLabel [71], a user-friendly interface for simulating spin-label dynamic data based on Easyspin is available from http:easyspin.org/forum.

Simulations are suitable to obtain τ_c for a certain spectrum and use it for quantitative comparison to another spectrum, but simulations are absolutely necessary for relative quantification when two or more species with different mobilities are present in the same sample/spectrum. As an illustrative example, we review the EPR study on the first enzyme

known to be intrinsically disordered [68]. In the article, the authors study the flexibility of UreG, a G-loop GTPase which is involved in the maturation of the nickel-containing urease, around the only native cysteine residue Cys68, labeled with MTSSL. The EPR spectrum under native conditions exhibit two major motional components that was possible to quantify by means of spectral simulations (see Fig. 5). One conformation, characterized by τ_c = 0.43 ns and estimated to be 50% of the total amount of enzyme has sharp and intense lines, whereas the other component accounting for the other 50% of the enzyme molecules is broader and much weaker in intensity, with τ_c = 5.5 ns. The fast component was associated with high flexibility and a lack of structure, while the slow component was attributed to protein folding in the region surrounding the label. In this example we are confronted with the dramatic intensity loss that takes place when the dynamics of the backbone is slowed down (note that in Fig. 3 the intensity of the spectra presented on the right column is multiplied by 20). The spectra of the two species overlap in such a way that the slow species might have remained unnoticed, since the only signs of it are weak humps at the feet of the three sharp nitroxide lines. The quantification of the species is based on the simulation of relatively subtle changes in the lineshape and intensity of the spectral features. This is due to the faster species being in the fast limit. Spectral changes due to decreasing correlation times in this regime are line narrowing, a $h_{(-1)}/h_{(0)}$ ratio closer to 1 and increasing intensity that dominates the whole spectrum, the line shape is not very sensitive to changes in dynamics in this range. The system is close to the isotropic limit, that is, we are taking a picture of an almost perfect ball.

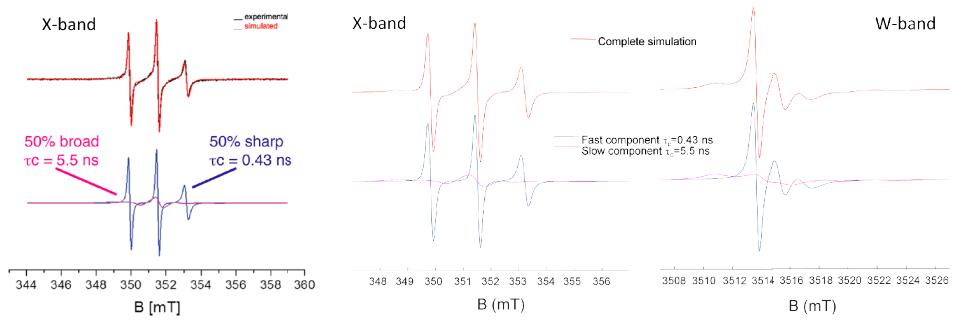

Figure 5. Experimental and simulated CW-EPR spectra of UreG. Left: X-band spectrum of UreG spin labeled at the position of the only cysteine present in the wild-type sequence, Cys68, under native conditions. The experimental spectrum (black) was simulated (red) with two species featuring different mobility. The fast component was fitted with correlation time 0.43 ns and the slow component with 5.5 ns. Note the difference in intensity of both contributions although their population is equal. **Center**: X-band simulation of the published spectrum using the reported parameters. **Right**: W-band simulation with identical parameters. Note that the broad component is now more visible in the spectrum. Left panel reproduced with permission from [68]

One idea that has given good results for spin labeled proteins [63], but, for now, only hypothesized with simulations for IDPs [72] is to decrease the exposure time of our camera, that is, use a higher microwave frequency. In the center and right panels of Fig. 5, X- and W-Band CW-EPR simulations by the author are presented for the two species found in [68],

details of the lineshapes are given to illustrate the higher sensitivity of the higher frequencies to spectra in the window of correlation times generally observed in IDPs. In the figure, the W-band features of the slow spectrum are more intense with respect to the ones of the fast component than at X-band. This is due to the higher anisotropy of the nitroxide spectrum at W-band magnetic fields.

Spin Label Packing and Oxygen/Quencher Accessibility.

When two or more unpaired electrons are in close proximity their orbitals may overlap, which leads to spin exchange interaction or coupling of the spins either in a parallel or antiparalell fashion. The effect of the exchange interaction on nitroxide free radicals in liquids is, for small spin exchange energies compared to the hyperfine coupling, to broaden the lines and move them toward the center of the spectrum. For exchange energies higher than the hyperfine coupling the lines broaden further and coalesce into one broad line, which narrows for even stronger exchange couplings [73]. On the other hand, the effect of this interaction decreases very rapidly when the distance between labels increases and, generally, one can safely neglect it when the distance between the spins is longer than 15 Å.

Another manifestation of the spin exchange interaction is the broadening and electron spin relaxation enhancement brought by collisions with other paramagnetic molecules present in the liquid solution. For example, oxygen is a paramagnetic molecule with a triplet ground state that diffuses in water and even better in lipid membranes due to its apolar character, it increases nitroxide relaxation rates via Heisenberg exchange proportionally to its concentration [74]. The same effect is obtained by other water soluble quenchers like NiEDDTA. Therefore, observing the effect of the different quenchers on the electron spin relaxation, one can obtain the exposure of a labeled residue to the water solution, to the lipid bilayer, or its inaccessibility due to burial into the protein. The spin-lattice relaxation can be measured directly using pulse methods, or via power saturation curves of the CW-EPR spectrum.

The study by Langen and coworkers [75, 76] provides a very nice example of how this interaction yielded useful information on the structure of α-synuclein aggregates. This protein in water solution and the mononeric state is intrinsically disordered but it acquires helical structure in contact with lipid bilayers [77-79]. Upon aggregation, plays an important role in the pathogenesis of Parkinson's and other neurodegenerative diseases [80]. In their article, they performed CW-EPR experiments with a remarkably exhaustive collection of single cysteine mutants of a C-terminal truncation mutant of α-synuclein. This variant is more prone to aggregation but forms fibrils with a highly similar morphology to that of the wild-type protein. The authors performed a high-resolution scan of the protein aggregates by labeling, one by one, every single amino acid. As shown in Fig. 6, fibril formation induced important changes in the spectrum of the singly labeled mutants in the N-terminal domain of the protein and from the 99^{th} amino acid, which revealed several components of varying mobility, from heavily immobilized to highly dynamic. The changes are more striking in the central region (core) of the protein where the spectrum is defined by a broad single EPR line as a result of the

exchange interaction resulting from a large number of spin labels coming into contact tightly packed together.

In the same study, the authors performed O_2 accessibility measurements on the side chain (Π) of fibrils of α-synuclein mutants labeled with a nitroxide in 25% of the units using the power saturation method [13, 81]. For that, EPR spectra were measured at room temperature as a function of the microwave power in the presence of pure O_2 and N_2 at atmospheric pressure. Although it is not clear from the paper, this is most conveniently done using a capillary of the gas-permeable plastic TPX. The intensities of the central line were plotted as a function of the microwave power of the experiment to obtain the parameter $P_{1/2}$, the power at which the signal has half the intensity it would have for infinitely fast relaxation. The adimensional parameter Π is obtained by dividing $\Delta P'_{1/2}$, defined as the difference between $P_{1/2}$ in O_2 and N_2 divided by the linewidth of the central line in the absence of saturation, by $P'_{1/2}$ of a reference sample, for example crystalline DPPH (2,2-diphenyl-1-picrylhydrazyl) [82]. The results are displayed in the right axis of Fig. 6.C that shows also the mobility parameter ΔH_0^{-1}, the inverse of the central line width, as a function of the residue number. From the plot, it is clear that the residues displaying less restricted mobility also have higher O_2 accessibility. Moreover, although the O_2 accessibility is generally low in the core region of the protein, small oscillating changes are observed with a periodicity of 2 in several regions. The periodicity in accessibility is often used to asses secondary structure in proteins and alternating values of Π is the sort of periodicity observed in soluble globular protein β-sheets wherein exposed and buried residues alternate. Therefore, the results confirmed the indications of protein β-sheet formation with tight packing interactions on both sides of the sheet, probably being one of them more accessible to O_2.

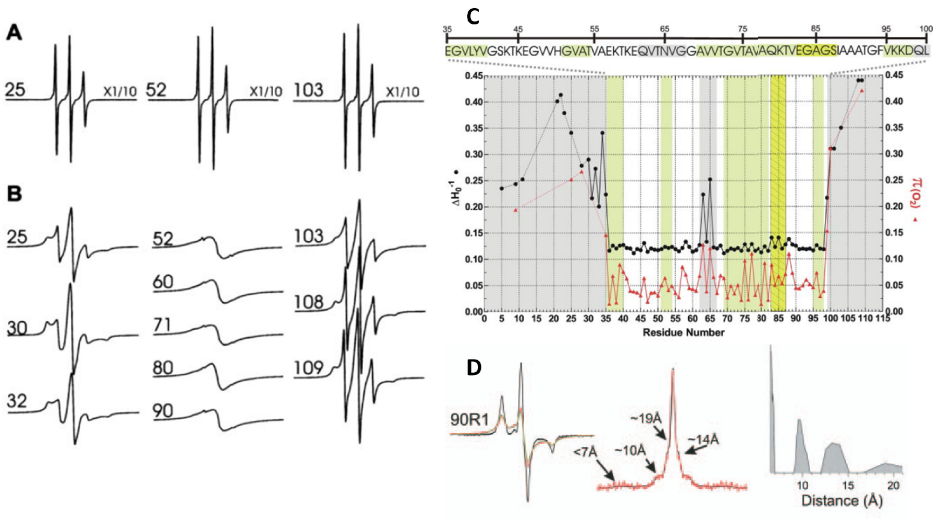

Figure 6. EPR of spin labeled α-synuclein. A. EPR spectra of single mutants of α-synuclein in the soluble form with a spin labeled cysteine at the positions indicated. **B**. EPR spectra of the designated spin labeled derivatives in fibril form. **C**. Illustration of EPR line width (ΔH0-1) and O_2 accessibility (Π) as a function of the residue number in fibrils containing 25% of R1. **D**. **Left**:

Low temperature EPR spectrum of truncated α-synuclein labeled at the position 90 in fibrils labeled with 40% R1 (red) and fibrils labeled with 10% R1 (black). **Center**: Deconvolution of the two aforementioned spectra in the frequency domain. **Right**: Fitting of the experimentally obtained broadening function to a set of Pake patterns. Adapted from [75]

With these experiments it was concluded that in α-synuclein fibrils are formed by a parallel, in-register stacking of the core region of the protein (35-99 aa) with multiple protein units clustered together. The distance between protein units was determined to be 4.7-4.8 Å based on the dipole interaction, which is reviewed in the next sections.

Determination of Distance Distributions Between Spin-Labels

One of the mayor features of EPR in relation to the study of IDPs in particular, and biomolecules in general, is the ability of the technique to, always in combination with site-directed spin labeling, obtain the distance between two paramagnetic centers. The measurements of distance distributions allows for recognizing and modeling disordered regions in a biomolecule. The physical principle behind distance determination is the dipole-dipole interaction. Just like classical magnetic dipoles, the magnetic interaction of two localized electron spins with magnetic moments μ_1 and μ_2 that are aligned parallel to an external magnetic field corresponds to the following interaction energy:

$$E_{dd} = -\frac{\mu_0}{4\pi} g_1 g_2 \mu_B^2 \frac{1}{r^3}(3cos^2\theta - 1) = \omega_\perp(1 - 3cos^2\theta) \quad \text{(Eq. 1)}$$

where the magnetic moments of the two paramagnetic centers are $\mu_1 = g_1\mu_B$ y $\mu_2 = g_2\mu_B$, μ_B is the Bohr magneton and θ is the angle between the magnetic field and the direction of the inter-spin vector $\vec{r}$. As denoted in the formula, the interaction is inversely proportional to the cube of the distance between the two point dipoles. The value of the dipole-dipole coupling, $\omega_\perp$, between two nitroxide radicals (g-values around the one of the free electron) is about 52 MHz for an inter-spin distance of 1 nm, for 10 nm it is reduced by three orders of magnitude.

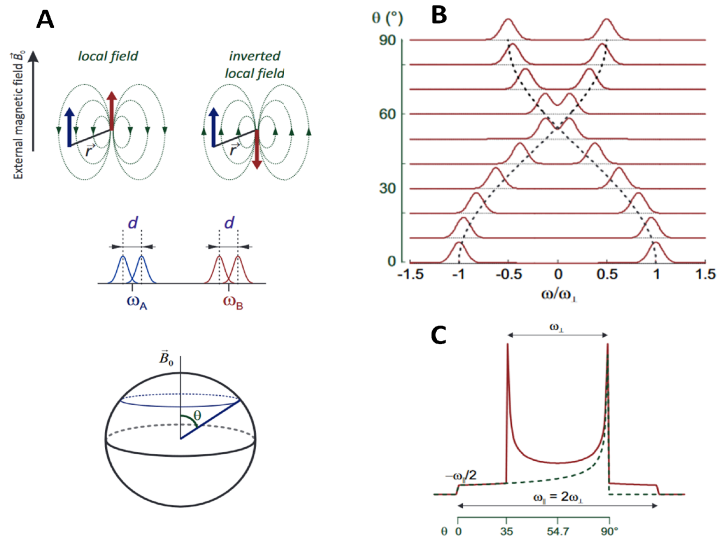

Figure 7. Spin dipole-dipole interaction. A. **Top**: diagram indicating how the local magnetic field of an electron changes with the spin-flip of a neighboring electron. **Center**: The EPR resonance absorption line of the two interacting electrons is split by the dipole-dipole interaction. **Bottom**: The angle between the external magnetic field and the inter-spin direction is represented in the sphere of all possible orientations. **B**. Rotational pattern of the dipolar coupling, dipole-dipole splitting as a function of the inter-spin vector orientation. **C**. Pake pattern resulting from the sum of all possible dipole-dipole inter-spin vector orientations. Figure kindly supplied by Gunnar Jeschke.

In the top diagram of Fig. 7.A. the influence of the spin state of the neighboring label (blue) on the local field of the measured (red) spin is displayed. Due to this magnetic interaction, for a certain orientation between the external magnetic field and the interspin direction, the EPR transitions of the two spins are split as represented in the center panel of Fig. 7.A. Since the dipole-dipole interaction depends on the angle θ, the splitting varies with θ as shown in Fig. 7.B. As a consequence of the presence of all possible molecular orientations in a frozen solution sample, each of the split lines broadens with a powder pattern as shown in Fig. 7.C. This is the so-called Pake pattern. Most often, the Pake pattern is not observed in the spectrum because other anisotropic interactions are larger than the dipole interaction.

If the weak coupling condition is fulfilled ($d < |\omega_A - \omega_B|$), the EPR line is the convolution of the Pake pattern with the lineshape in the absence of interaction between the dipoles. If this line shape is known, the Pake pattern, and the distance, can be obtained by de-convolution of the CW-EPR spectrum [83]. This kind of study must be performed at low temperature, in the "rigid limit" T < 200 K, in order to avoid the dipole-dipole interaction to be averaged out by the molecular motion. Note also that the interaction between dipoles can be measured between labels in the same molecule (intramolecular distance) or between labels in different molecules

(intermolecular distance) and occurs between identical labels but also between different labels (orthogonal labeling). To safely obtain distance information from spin labels, the exchange interaction between labels has to be negligible and the distance between labels much larger than the spatial distribution of the label position. This is fulfilled for mean distances larger than 15 Å approximately.

Coming back to the study of nitroxide labeled α-synuclein fibrils performed by Chen at al. [75] and summarized in Fig.6, we find an illustrative example on how the distance between β-sheets was obtained using CW-EPR (Figure 6.D). As it was already mentioned, the CW-EPR spectrum of fibrils constructed with singly labeled monomers of the protein was dominated by exchange interactions due to the close packing among labels of the parallel monomers in the aggregate. From these spectra it is difficult to obtain an estimate of the exact distance between labels, since the exchange interaction is difficult to interpret in terms of geometric distance and the dipole interaction is obscured by the exchange interaction. Again, a good strategy is to "dilute" the spin system by co-precipitating the protein attached to the spin label with the protein where the label was substituted by its diamagnetic analogue. The authors performed at 233 K a series of spin dilution experiments with various mixtures of R1 and its diamagnetic analogue R1' to increase the distance between spin labels and avoid the effects of the spin exchange interaction and recover, at least for some of the labels, the three-line EPR spectrum characteristic of the hyperfine coupling with restricted mobility. They found that starting from 50% of spin labeled protein, the spectra are dominated by the exchange interaction, while for percentages lower than that, dipole-dipole interaction was dominating the spectral broadening. In order to recover the Pake-pattern broadening function, which could be used to obtain the interspin distances, they deconvoluted the spectra of α-synuclein at 40% R1 (dipolar-broadened) with the ones obtained for 10% R1 (less dipolar broadening). The results for the protein with the spin label placed at position 90 of the sequence are displayed in figure 6.D left, where it becomes clear from the several peaks and shoulders of the broadening function in the frequency domain that there are several sets of distances. The retrieval of the distance distribution function (Fig. 6.D right) shows distance peaks at 10, 14 and 19 Å, which correspond approximately to the distance between three, four and five β-strands measured in fiber diffraction studies [84]. As illustrated above, distance measurements in the range 10 – 20 Å can be extracted from CW-EPR measurements of spin labeled proteins. For distances longer than 20 – 25 Å, the dipole-dipole coupling is normally so small that broadening caused by spin-spin interactions cannot be detected since other mechanisms, like non-resolved hyperfine splittings or g- and A-strains, dominate and generate a much broader linewidth. form

Distance measurement between labels using CW-EPR is limited in the case the pairs of labels are "diluted" into a background of labels that are not paired, for example when measuring the distance within a dimer of a singly labeled protein when the proportion of dimers is lower than 40%, or when the labeling efficiency of a doubly labeled protein is lower than 60%. This limitation is caused by the fact that all labels contribute to the CW-EPR signal and obscure subtle broadenings produced only by a fraction of the pairs. Note that using deconvolution methods requires necessarily the spectrum of the non-interacting species and neglects potential orientation selection effects, that is, correlation of the interspin direction and the molecular frame. In case of broad distance distributions, as to be expected for IDPs, the risk is

that part of the distribution falls out of the sensitive range of the method. The use of complicated model functions to fit distance distributions is to be avoided since the number of parameters rise up fast.

Many of these limitations can be overcome with pulsed methods for distance determination between spin centers.

Distance Determination with Pulsed Methods

The use of pulsed EPR methods allows manipulating the magnetization with high-power microwave pulses. Reversing the effects of inhomogeneous line broadening is possible through the formation and detection of electron spin echoes [85]. There are several pulsed dipolar spectroscopy methods in the literature: Double-quantum EPR (DQ-EPR) [86, 87], SIFTER (SIngle-Frequency TEchnique for refocusing dipolar couplings) [88, 89], DEER (also known as PELDOR [90, 91], Pulsed ELectron-electron DOuble Resonance) and RIDME [92]. From them, the one more widely used at the moment is the four-pulse version of DEER [9].

In this experiment, two interacting spins resonating at a different frequency are manipulated independently by pulses of different microwave frequency. The pulse sequence is shown in Fig. 8, the first two pulses at the resonance frequency of the observed spins (spins A in Fig. 7) produce a Hahn echo that is refocused by the fourth pulse after the evolution time *t*. In the meantime, a π pulse at the resonance frequency of the interacting spins (pump pulse) inverts them, changing thereby the resonance frequency of the observed spins, which will not refocus unless the evolution time from that moment multiplied by frequency change (dipolar frequency) is a multiple of 2π. When the pump pulse position is swept during the evolution time, an oscillating signal is detected. The information of the distance between the spin centers is encoded in the frequency of the oscillation. For this technique to work, the two spins need to be manipulated independently, that is, they have to have different resonance frequency. The spectrum of nitroxides spans a 180 MHz spectral width and therefore it is possible to allocate two non-overlapping pulses, the pump-pulse is normally set at the maximum of the nitroxide spectrum, where all molecular orientations contribute and the observer-pulse is set to excite the spins at the low-field end of the spectrum (molecular axis along the external magnetic field). As noted above, the equally likely occurrence of every molecular orientation in a frozen sample, results for X- and Q-band DEER spectra in a full Pake pattern in the frequency domain. Gd-Gd distance between gadolinium spin labels and Gd-NO distances can also be measured with this technique without noticeable orientation selection effects although severely decreased modulation depth [36, 37, 93, 94].

However, not only the desired signal is recorded in the spectrum; if the protein concentration is high enough, there is a considerable probability that different proteins, randomly distributed in space, interact among themselves if they are close enough. These random interactions will be recorded as well, as the so-called background factor. For a certain interspin distance *r*, the normalized DEER signal has the mathematical form:

$$\frac{V(t)}{V(0)} = F(t)B(t) = \underbrace{F(0)\int_0^{\pi/2}(1-\lambda[1-cos\{\omega_\perp(r)(3cos^2\theta-1)\}t])sin\theta d\theta}_{\tilde{F}(t)} \cdot \underbrace{e^{-(kt)^{D/3}}}_{B(t)} \quad \text{(Eq. 2)}$$

where *F* is the form factor due to the intramolecular contribution with distance *r*, and *B* is the background factor. In this formula, the dependence of the dipole-dipole coupling on the angle θ between the spin-spin vector and the direction of the magnetic field is explicit. Again, all orientations of the interspin vector are possible in a frozen solution and the different contributions need to be summed up (integration over θ). The background factor is normally approximated by a stretched exponential function. For a homogeneous spatial distribution of proteins in three dimensions, as it is to be expected for soluble proteins like IDPs, the dimensionality index D is found to be close to 3. The form factor can be obtained by fitting the background factor using the last part of the DEER trace (see Fig. 8) and dividing the trace by the fit. Background factors can also be obtained experimentally from singly labeled samples. After renormalization, there is a non-modulated contribution to the form factor given by non-interacting spins that can be subtracted to obtain the modulated contribution bearing the distance information. Unlike what happens with CW-EPR experiments, non-interacting spins do not interfere with the effect produced by interacting spins.

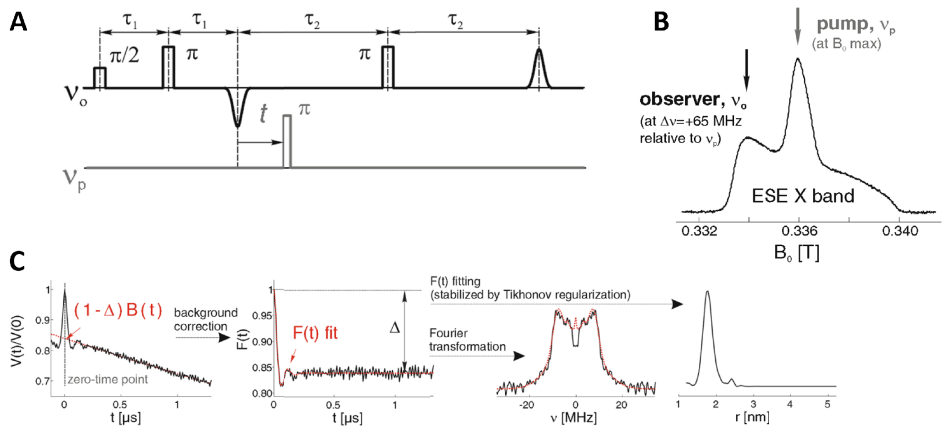

Figure 8. A. **DEER/PELDOR experiment.** DEER pulse sequence at the frequencies of the observer (ν_0) and pump spins (ν_p). **B**. Echo-induced EPR spectrum of a nitroxide label with the position of the observer and pump spins. **C**. Data processing of the time trace with DeerAnalysis. First panel (left): Normalized and phase corrected raw experiment, second panel: Form factor after background correction, third panel: Frequency-domain dipolar spectrum, fourth panel (right): Distance distribution. Adapted from [95]

DEER experiments have to be performed in the frozen state; agents like glycerol are normally used to obtain a glass upon freezing. For nitroxides, optimal values for the relevant relaxation time T_2 occur at a temperature of about 50 K. Further extension of T_2, and therefore longer dipolar evolution traces can be obtained by deuteration of the sample. Using a high-power Q-band spectrometer at 50 K allows measuring distance distributions from 1.8 up to 10 nm in deuterated soluble proteins [9]. In some reported cases this limit is extended to 16 nm [96]. The measurement of longer distances is more challenging as the interaction between spins is correspondingly weaker. A weaker interaction will produce slower oscillations in the form

factor, which need the measurement of longer evolution times in the experiment. This yields to a reduction of the signal due to transverse relaxation. Moreover, the longer the distance the harder is to distinguish it from the background contribution for a certain protein concentration. In this case, a decrement in the protein concentration is advised leading to a further reduction of the signal.

Analysis of the form factor to retrieve the distance distribution between the spins is not obvious because small variations in the input data (time trace) can lead to large differences distance distribution. Tikonov regularization is a method that stabilizes the solution by not only searching for a good RSMD but also a smooth solution [97-99]. This method is a solid way of obtaining distance distributions from experimental DEER traces without assuming a specific model for the shape of the distribution. Limitations arise when sharp and broad distances are present in the data [100]. New approaches combine denoising and singular value decomposition [101, 102], neural networks [103] or regularization methods based on Bregman iterations [104].

DEERAnalysis [105] is a widely spread, user friendly tool for processing and analysis of DEER experimental traces available free of charge as a MATLAB toolbox from the website of the developers (https://epr.ethz.ch/software.html). An example illustrating the processing and analysis of a DEER trace is shown in Fig. 8. Evaluating uncertainty of a distance distribution is absolutely necessary as the output of the analysis is very dependent of the signal to noise of the experimental trace and the fit of the background function [106, 107]. DeerAnalysis includes a validation module to check the reliability of the different features in the distance distribution [108].

For IDPs, distance distributions are expected to be very broad, reflecting the disorder of the structure. In this case, no oscillations are to be observed in the trace but a steady decrease (more or less steep for shorter or longer distances) that has to be separated from the background decay. For such broad distance distributions the analysis and their subsequent interpretation becomes even more challenging since the use of small regularization parameters is not appropriate for broad distributions and large regularization parameters could hide details from the distribution. Some authors fit their distributions to a predefined model, usually Gaussians [109], although this fit will fail to reflect any real asymmetry in the distance distribution.

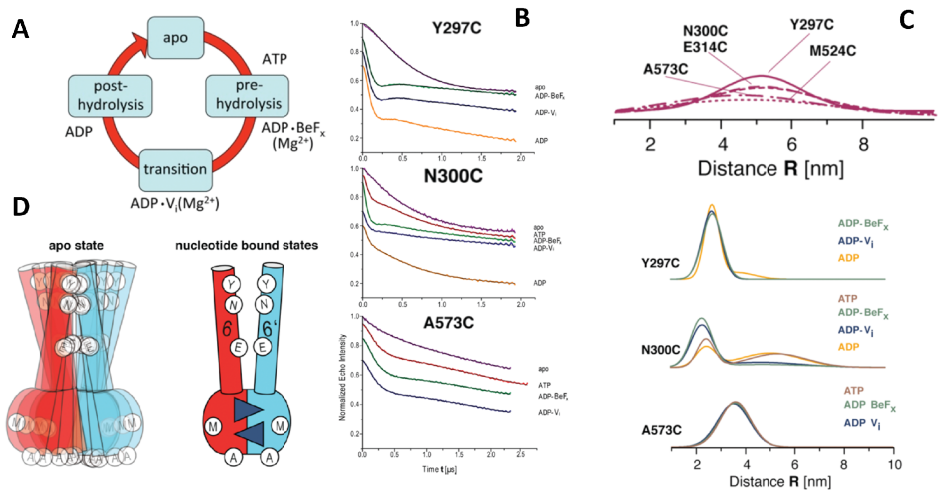

Figure 9. Pulse EPR reveals flexibility in the apo state of LmrA transporter. A. Schematic cycle of the transporter with the states isolated for the study **B**. Raw DEER data of some of the mutants for the different states. In contrast to the nucleotide-bound states, the apo-state does not show oscillations due to the broad distance distribution. **C**. Distance distributions obtained from DEER data considering Gaussian models in the apo state (up) or nucleotide-bound states (down). **D**. Sketch of the protein dimer. Adapted from [110]

In Fig. 9 an example is presented of a site-directed spin labeling study combined with DEER in which the traces are fitted by bimodal Gaussian distributions. The authors examined a member of ATP binding cassette transporter superfamily, the protein LmrA, a homodimeric multidrug transporter [110]. They spin labeled five positions, two in the nucleotide binding domain of the protein and three in one of the transmembrane helixes, helix 6, and prepared the protein in four different states of its transport cycle by addition of different substrates and substrate analogues: apo-state (no nucleotide bound), pre-hydrolysis (bound to a nucleotide ADP-BeF_x), transition (with the inhibitor ADP-Vi) and post-hydrolysis (bound ADP) (Fig 9.A). The raw time traces are shown in Fig. 9.B. For the five mutants, the nucleotide states show dipolar oscillations due to the intramolecular interaction between spin labels. On the other hand, only a monotonic decay was observed for all mutants in the apo-state that is more or less pronounced depending on the mutant but with no signs of oscillations. This can already be interpreted as a sign of a broad distance distribution. Once the intermolecular decay was taken into account the data were fitted either with a single or double Gaussian distance distribution (Fig. 9.C). Although the quality of the fit was not given, the distributions show a significant narrowing on going from the apo to any of the nucleotide bound states, which show very similar inter-spin distances. This fact was interpreted by the authors as a highly flexible apo-state where large amplitude domain fluctuations (disorder) take place and is captured upon freezing the whole ensemble to low temperature EPR conditions (40 K in this case). The authors discuss that flexibility/disorder might be an important functional prerequisite for recognition of a large variety of substrates.

A second interesting example where DEER distance measurements between paramagnetic labels were used to monitor proteins in a disordered state is the refolding study of the mayor light-harvesting complex protein (LHCII) of photosynthetic plants [21, 111]. When the detergent-solubilized protein is mixed with a combination of chlorophylls *a* and *b* and carotenoids, the apoprotein folds and binds its pigments *in vitro*. Distance constraints from pulse EPR were used to study protein folding and pigment binding in a time-resolved manner by shock-freezing the sample at certain times after mixing. Intra-molecular distances were measured before folding and at various time points in the folding process and compared with the ones in the fully folded and assembled LHCII. Double mutants were designed to place spin labels at both ends of each of the transmembrane helixes and between the lumenal (and stromal) ends of two of the three helixes. Fig. 10.A illustrates the steps of DEER trace processing with the labels at positions 90 and 196 in the fully reconstituted protein. For shock-frozen samples reporting about the kinetic of the folding process, the protein amount in the sample tubes was considerably reduced. Due to the higher sensitivity provided by the Q-band study [111], DEER traces were long enough to retrieve reliable distance distributions. On the other hand, in the previous X-band study [21], it was only possible to perform the experiments with short dipolar evolution times (1.5 µs), which partially suppresses long distances due to imperfect background correction. Protein folding was therefore monitored by focusing on the disappearance of large frequencies (short distances) from the dipolar spectra (see Fig. 10). The quantification of the folding kinetics from dipolar spectra was found more reliable since large dipolar frequencies can be detected even for short evolution times and the computation of dipolar spectra does not amplify noise-related distortions, unlike what is found for the computation of distance distributions. These time resolved EPR studies allowed concluding that most of the folding of the three transmembrane alpha helices precedes their apposition into the final tertiary structure. However, their formation follows different kinetics, even extending into a final phase during which much of the condensation of the pigment-protein structure occurs.

Figure 10. Study of LHCII folding. A. DEER data analysis of the purified mutant 90/196 after reconstitution. **Top-left**: raw data of the doubly labeled mutant and a mixture of single mutants 196 and 90. Top-right data after background correction. **Bottom-left**: Dipolar spectrum. **Bottom-right**: Distance distribution. **B**. Assembly of LHCII as monitored by DEER measurements on 106/160 and 90/196. Time traces were short (1,400 ns cut off time). Left: DEER-dipolar spectra at three different folding times. Frequencies higher than the isosbestic point (arrow) are shaded and integrated. Right: Time-dependent decrease of the high-frequency integral in dipolar spectra obtained for each mutant at different freezing times. **C**. Structure of LHCII based on the crystal structure (PDB ID code 2BHW). Adapted from [21]

The last revised example of distance measurements using DEER refers to the protein α-synuclein that was mentioned above. The aim of the study was to compare the conformation/flexibility of the protein in vitro with the one of the protein in its native environment, the cell [112]. Single and double cysteine mutants of the protein were labeled with Gd-DOTA, chosen in order to survive the reducing environment in the cell. Gd-Gd (also Gd-NO) distance constraints at X- and Q-bands do not show any orientation selection effects and, albeit a few technicalities, the processing and subsequent interpretation of the data can be done using the same criteria as for NO-NO distance constraints. Consistent with the disordered nature of the protein, the DEER traces show no oscillations and the average distance between the labels is encoded in the slope of the form factor decay. The experiments show no mayor difference between the conformation of the protein in vitro (IDP) and the protein in the cell.

Integrating the Distance Constraints into a Structural Model.

In order to interpret correctly the outcome of distance measurements between labeled residues in terms of distances between the different points of the backbone where the label is attached, one has to take into account the specific nature of the labeled amino acid (normally cysteine) and the structure of the particular label, as well as the flexibility of the formed R1 side chain. One of the features of the spin labels that we have noted above is the flexibility, which, in one hand allows them to adapt to the landscape of the particular site with minimal alteration of its native structure, but on the other hand blurs the position of the electron spin due to conformation disorder of the spin label side chain. For accurate distance determination, the position of the electron spin has to be modeled; however, prediction of the conformational flexibility of the probe introduces uncertainty. One of the most popular approaches to account for this flexibility is to model the spin label using precomputed rotamer libraries with calculated probabilities for every possible conformer based on methods of molecular dynamics [113]. When a spin label is modeled into a particular position of the structure, only the conformers that do not collide with the protein will be selected. One then calculates the partition function, which is related to how much conformational freedom the probe has on the site, in order to obtain the probability of every individual conformer. The open-source package MMM (http://www.epr.ethz.ch/software/index), also a toolbox for MATLAB, has implemented this approach and incorporates a precalculated library of rotamers for the most common nitroxide and gadolidium labels [12]. With the probabilities for individual rotamers given by MMM, the average position of the spin probe is calculated for every labeled site. The software also allows for calculation of distance distributions and DEER trace computations of sites labeled *in silico* from a certain protein structure. With these tools, mean distances between two MTSSL spin labels can be predicted with a standard deviation of about 2 Å if the backbone structure and other side chain conformations are known at a high resolution [19]. This limitation, together with the fact that EPR distance restrains are usually sparse precludes a full specification of structure determination at atomic resolution from EPR restraints only. Studies as systematic as the one performed in the α-synuclein study reviewed above [75] where the spin label was scanned along the protein residue by residue are very rare, EPR distance restraints are normally scarce due to the large effort behind mutating, expressing and purifying, spin labeling and measuring of every labeling position. Therefore, the best approach is to combine EPR distance constraints with structural information provided by other techniques and with modeling of the molecule.

MMM is prepared to integrate EPR constraints with atomistically resolved structures, secondary structure propensities (from sequence, NMR or EPR techniques), small angle x-ray scattering, homology modeling and elastic network models. In the case of intrinsically disordered proteins or domains, the idea of distance between atoms is invalid, and the useful information within the EPR distance distributions is the average and width of the ensemble of conformations. With several of those distance restraints one can attempt to model an ensemble of structures than fulfill all of the restraints obtained experimentally. In this case MMM provides a very useful tool, *Domain Ensemble Modeling* [12]. This tool generates the structure of a given protein sequence, either the whole protein or a protein segment, based on Montecarlo methods. Conformers are generated from pseudo-random backbone torsion angles consistent with the Ramachandran plot of the corresponding residue. The process of

checking the distance restraints is built in the structure construction routine, so that conformers that violate the restraints are rejected immediately. If a protein loop or segment is modeled, the algorithm starts generating the N-terminal residue and is steered towards their C-terminal anchor by a Montecarlo Metropolis approach [11, 12]. Subsequently, side chains are generated and clash tests are performed. Secondary structure restraints, bilayer immersion depth and distance restraints are implemented. The tool generated output is the user predefined number of structures compliant with the restraints. It also provides very useful information about the number of models rejected and the reason for rejection (restraints violation, clashes within the domain or with the protein, etc). The comparison of the output ensemble with a run with no restraints can give an idea of how disordered the protein or domain really is. The approach has been tested with simulated restraints for well-defined structures and for published ensembles of intrinsically disordered proteins to see whether/when the uncertainty is due to lack of experimental restraints and when is due to intrinsic disorder. Both situations can be distinguished if enough distance distribution restraints are available [11].

ACKNOWLEDGEMENTS

I would like to thank Prof. Gunnar Jeschke and his entire present and past group for the long-standing collaboration and fruitful discussions. I would like also to acknowledge Tony Famulary for his support with the chemical structures. The financial contributions from MINECO (CTQ2015-64486-R), Gobierno de Aragón (E35_17R) and Fondo Social Europeo-"Construyendo Europa desde Aragón" are greatly appreciated.

REFERENCES

1. Dunker, A.K. and Z. Obradovic, *The protein trinity - linking function and disorder.* Nature Biotechnology, 2001. **19**(9): p. 805-806.
2. Uversky, V.N., *Intrinsically disordered proteins from A to Z.* International Journal of Biochemistry & Cell Biology, 2011. **43**(8): p. 1090-1103.
3. Uversky, V.N. and A.K. Dunker, *Understanding protein non-folding.* Biochimica Et Biophysica Acta-Proteins and Proteomics, 2010. **1804**(6): p. 1231-1264.
4. Chouard, T., *Breaking the protein rules.* Nature, 2011. **471**(7337): p. 151-153.
5. Habchi, J., et al., *Introducing Protein Intrinsic Disorder.* Chemical Reviews, 2014. **114**(13): p. 6561-6588.
6. Drescher, M., *EPR in Protein Science Intrinsically Disordered Proteins.* Epr Spectroscopy: Applications in Chemistry and Biology, 2012. **321**: p. 91-119.
7. Le Breton, N., et al., *Exploring intrinsically disordered proteins using site-directed spin labeling electron paramagnetic resonance spectroscopy.* Frontiers in Molecular Biosciences, 2015. **2**(21).
8. Hubbell, W.L., et al., *Technological advances in site-directed spin labeling of proteins.* Current Opinion in Structural Biology, 2013. **23**(5): p. 725-733.
9. Jeschke, G., *DEER Distance Measurements on Proteins.* Annual Review of Physical Chemistry, Vol 63, 2012. **63**: p. 419-446.
10. Jeschke, G., *The contribution of modern EPR to structural biology.* Emerging Topics in Life Sciences, 2018. **2**: p. 9-18.

11. Jeschke, G., *Ensemble models of proteins and protein domains based on distance distribution restraints.* Proteins-Structure Function and Bioinformatics, 2016. **84**(4): p. 544-560.
12. Jeschke, G., *MMM: A toolbox for integrative structure modeling.* Protein Science, 2018. **27**(1): p. 76-85.
13. Altenbach, C., et al., *Structural Studies on Transmembrane Proteins .2. Spin Labeling of Bacteriorhodopsin Mutants at Unique Cysteines.* Biochemistry, 1989. **28**(19): p. 7806-7812.
14. Altenbach, C., et al., *Transmembrane Protein-Structure - Spin Labeling of Bacteriorhodopsin Mutants.* Science, 1990. **248**(4959): p. 1088-1092.
15. Couet, W.R., et al., *Influence of Chemical-Structure of Nitroxyl Spin Labels on Their Reduction by Ascorbic-Acid.* Tetrahedron, 1985. **41**(7): p. 1165-1172.
16. Paletta, J.T., et al., *Synthesis and Reduction Kinetics of Sterically Shielded Pyrrolidine Nitroxides.* Organic Letters, 2012. **14**(20): p. 5322-5325.
17. Bleicken, S., et al., *gem-Diethyl Pyrroline Nitroxide Spin Labels: Synthesis, EPR Characterization, Rotamer Libraries and Biocompatibility.* Chemistryopen, 2019. **8**(8): p. 1057-1065.
18. Karthikeyan, G., et al., *A Bioresistant Nitroxide Spin Label for In-Cell EPR Spectroscopy: In Vitro and In Oocytes Protein Structural Dynamics Studies.* Angewandte Chemie-International Edition, 2018. **57**(5): p. 1366-1370.
19. Jeschke, G., *Conformational dynamics and distribution of nitroxide spin labels.* Progress in Nuclear Magnetic Resonance Spectroscopy, 2013. **72**: p. 42-60.
20. Cattani, J., V. Subramaniam, and M. Drescher, *Room-temperature in-cell EPR spectroscopy: alpha-Synuclein disease variants remain intrinsically disordered in the cell.* Physical Chemistry Chemical Physics, 2017. **19**(28): p. 18147-18151.
21. Dockter, C., et al., *Refolding of the integral membrane protein light-harvesting complex II monitored by pulse EPR.* Proceedings of the National Academy of Sciences of the United States of America, 2009. **106**(44): p. 18485-18490.
22. Bordignon, E., *Site-Directed Spin Labeling of Membrane Proteins.* Epr Spectroscopy: Applications in Chemistry and Biology, 2012. **321**: p. 121-157.
23. Alonso-Garcia, N., et al., *Combination of X-ray crystallography, SAXS and DEER to obtain the structure of the FnIII-3,4 domains of integrin alpha 6 beta 4.* Acta Crystallographica Section D-Structural Biology, 2015. **71**: p. 969-985.
24. Mileo, E., et al., *Enlarging the Panoply of Site-Directed Spin Labeling Electron Paramagnetic Resonance (SDSL-EPR): Sensitive and Selective Spin-Labeling of Tyrosine Using an Isoindoline-Based Nitroxide.* Bioconjugate Chemistry, 2013. **24**(6): p. 1110-1117.
25. Steinhoff, H.J., et al., *2-Dimensional Diffusion of Small Molecules on Protein Surfaces - an Epr Study of the Restricted Translational Diffusion of Protein-Bound Spin Labels.* European Biophysics Journal with Biophysics Letters, 1991. **20**(5): p. 293-303.
26. Hideg, K., T. Kalai, and C.P. Sar, *Recent results in chemistry and biology of nitroxides.* Journal of Heterocyclic Chemistry, 2005. **42**(3): p. 437-450.
27. Fleissner, M.R., et al., *Site-directed spin labeling of a genetically encoded unnatural amino acid.* Proceedings of the National Academy of Sciences of the United States of America, 2009. **106**(51): p. 21637-21642.
28. Schmidt, M.J., et al., *A Genetically Encoded Spin Label for Electron Paramagnetic Resonance Distance Measurements.* Journal of the American Chemical Society, 2014. **136**(4): p. 1238-1241.
29. Rassat, A. and P. Rey, *Nitroxides. 23. Preparation of amino acid free radicals and their complex salts* Bulletin de la Societe Chimique de France, 1967. **3**: p. 815-818.

30. Toniolo, C., et al., *The Polypeptide 3(10)-Helix as a Template for Molecular Recognition Studies - Structural Characterization of a Side-Chain Functionalized Octapeptide.* Bioorganic & Medicinal Chemistry, 1995. **3**(9): p. 1211-1221.
31. Elsasser, C., et al., *Orientation of spin labels in de novo peptides.* Magnetic Resonance in Chemistry, 2005. **43**: p. S26-S33.
32. Becker, C.F.W., et al., *Incorporation of spin-labelled amino acids into proteins.* Magnetic Resonance in Chemistry, 2005. **43**: p. S34-S39.
33. Ritsch, I., et al., *Pulsed EPR Methods to Study Biomolecular Interactions.* Chimia, 2019. **73**(4): p. 268-276.
34. Gmeiner, C., et al., *Structural information of PTBP1/EMCV complex by combining orthogonal spin labelling with pulse EPR.* European Biophysics Journal with Biophysics Letters, 2017. **46**: p. S140-S140.
35. Gmeiner, C., et al., *Orthogonal Tyrosine and Cysteine Site-Directed Spin Labeling for Dipolar Pulse EPR Spectroscopy on Proteins.* Journal of Physical Chemistry Letters, 2017. **8**(19): p. 4852-4857.
36. Garbuio, L., et al., *Gd(III) complexes for electron-electron dipolar spectroscopy: Effects of deuteration, pH and zero field splitting.* Journal of Magnetic Resonance, 2015. **259**: p. 163-173.
37. Potapov, A., et al., *Nanometer-Scale Distance Measurements in Proteins Using Gd3+ Spin Labeling.* Journal of the American Chemical Society, 2010. **132**(26): p. 9040-9048.
38. Abdelkader, E.H., et al., *A New Gd3+ Spin Label for Gd3+-Gd3+ Distance Measurements in Proteins Produces Narrow Distance Distributions.* Journal of Physical Chemistry Letters, 2015. **6**(24): p. 5016-5021.
39. Raitsimring, A.M., et al., *Gd3+ complexes as potential spin labels for high field pulsed EPR distance measurements.* Journal of the American Chemical Society, 2007. **129**(46): p. 14138-+.
40. Song, Y., et al., *Pulsed dipolar spectroscopy distance measurements in biomacromolecules labeled with Gd(III) markers.* Journal of Magnetic Resonance, 2011. **210**(1): p. 59-68.
41. Kaminker, I., et al., *Spectroscopic selection of distance measurements in a protein dimer with mixed nitroxide and Gd3+ spin labels.* Physical Chemistry Chemical Physics, 2012. **14**(13): p. 4355-4358.
42. Lueders, P., G. Jeschke, and M. Yulikov, *Double Electron-Electron Resonance Measured Between Gd3+ Ions and Nitroxide Radicals.* Journal of Physical Chemistry Letters, 2011. **2**(6): p. 604-609.
43. Martorana, A., et al., *Probing Protein Conformation in Cells by EPR Distance Measurements using Gd3+ Spin Labeling.* Journal of the American Chemical Society, 2014. **136**(38): p. 13458-13465.
44. Qi, M., et al., *Gd(III)-PyMTA Label Is Suitable for In-Cell EPR.* Journal of the American Chemical Society, 2014. **136**(43): p. 15366-15378.
45. Roser, P., et al., *Site-directed spin labeling of proteins for distance measurements in vitro and in cells.* Organic & Biomolecular Chemistry, 2016. **14**(24): p. 5468-5476.
46. Theillet, F.X., et al., *Structural disorder of monomeric alpha-synuclein persists in mammalian cells.* Nature, 2016. **530**(7588): p. 45-+.
47. Yang, Y., et al., *A Reactive, Rigid Gd-III Labeling Tag for In-Cell EPR Distance Measurements in Proteins.* Angewandte Chemie-International Edition, 2017. **56**(11): p. 2914-2918.
48. Banerjee, D., et al., *Nanometer-Range Distance Measurement in a Protein Using Mn2+ Tags.* Journal of Physical Chemistry Letters, 2012. **3**(2): p. 157-160.
49. Narr, E., A. Godt, and G. Jeschke, *Selective measurements of a nitroxide-nitroxide separation of 5 nm and a nitroxide-copper separation of 2.5 nm in a terpyridine-based*

copper(II) complex by pulse EPR spectroscopy. Angewandte Chemie-International Edition, 2002. **41**(20): p. 3907-3910.
50. Merz, G.E., et al., *Site-Specific Incorporation of a Cu2+ Spin Label into Proteins for Measuring Distances by Pulsed Dipolar Electron Spin Resonance Spectroscopy.* Journal of Physical Chemistry B, 2018. **122**(41): p. 9443-9451.
51. Bode, B.E., et al., *PELDOR measurements on a nitroxide-labeled Cu(II) porphyrin: Orientation selection, spin-density distribution, and conformational flexibility.* Journal of Physical Chemistry A, 2008. **112**(23): p. 5064-5073.
52. Kay, C.W.M., et al., *Pulsed ELDOR determination of the intramolecular distance between the metal binding sites in dicupric human serum transferrin and lactoferrin.* Journal of the American Chemical Society, 2007. **129**(16): p. 4868-+.
53. Joseph, B., et al., *Selective High-Resolution Detection of Membrane Protein-Ligand Interaction in Native Membranes Using Trityl-Nitroxide PELDOR.* Angewandte Chemie-International Edition, 2016. **55**(38): p. 11538-11542.
54. Yang, Z.Y., et al., *Pulsed ESR Dipolar Spectroscopy for Distance Measurements in Immobilized Spin Labeled Proteins in Liquid Solution.* Journal of the American Chemical Society, 2012. **134**(24): p. 9950-9952.
55. Stoll, S. and A. Schweiger, *EasySpin: Simulating CW ESR Spectra*, in *Biological Magnetic Resonance*, M.A. Hemminga and L.J. Berliner, Editors. 2007, Springer: New York. p. 299-321.
56. Schneider, D.J. and J.H. Freed, *Calculating Slow Motional Magnetic Resonance Spectra. A user's guide*, in *Biological Magentic Resonance*, L.J. Berliner and J. Reuben, Editors. 1976, Springer: New York. p. 1-76.
57. Mchaourab, H.S., et al., *Motion of spin-labeled side chains in T4 lysozyme, correlation with protein structure and dynamics.* Biochemistry, 1996. **35**(24): p. 7692-7704.
58. Qin, P.Z., et al., *Monitoring RNA base structure and dynamics using site-directed spin labeling.* Biochemistry, 2003. **42**(22): p. 6772-6783.
59. Hubbell, W.L., D.S. Cafiso, and C. Altenbach, *Identifying conformational changes with site-directed spin labeling.* Nature Structural Biology, 2000. **7**(9): p. 735-739.
60. Hubbell, W.L., et al., *Watching proteins move using site-directed spin labeling.* Structure, 1996. **4**(7): p. 779-783.
61. Perozo, E., D.M. Cortes, and L.G. Cuello, *Three-dimensional architecture and gating mechanism of a K+ channel studied by EPR spectroscopy.* Nature Structural Biology, 1998. **5**(6): p. 459-469.
62. Columbus, L. and W.L. Hubbell, *A new spin on protein dynamics.* Trends in Biochemical Sciences, 2002. **27**(6): p. 288-295.
63. Barnes, J.P., et al., *A multifrequency electron spin resonance study of T4 lysozyme dynamics.* Biophysical Journal, 1999. **76**(6): p. 3298-3306.
64. Steinhoff, H.J. and W.L. Hubbell, *Calculation of electron paramagnetic resonance spectra from Brownian dynamics trajectories: Application to nitroxide side chains in proteins.* Biophysical Journal, 1996. **71**(4): p. 2201-2212.
65. Steinhoff, H.J., et al., *Molecular dynamics simulation and EPR spectroscopy of nitroxide side chains in bacteriorhodopsin.* Journal of Molecular Liquids, 2000. **84**(1): p. 17-27.
66. Bordignon, E. and H.J. Steinhoff, *Membrane Protein Structure and Dynamics Studied by Site-Directed Spin-Labeling ESR*, in *ESR Spectroscopy in Membrane Biophysics. Biological Magnetic Resonance.*, L.J. Berliner, Editor. 2007, Springer. p. 129-164.
67. Pirman, N.L. and G.E. Fanucci, *Investigation of the Intrinsically Disordered Protein IA3 by Multiple SDSL-EPR Techniques.* Biophysical Journal, 2010. **98**(3): p. 257a-257a.
68. Palombo, M., et al., *The relationship between folding and activity in UreG, an intrinsically disordered enzyme.* Scientific Reports, 2017. **7**.
69. Ranaldi, S., et al., *Amplitude of Pancreatic Lipase Lid Opening in Solution and Identification of Spin Label Conformational Subensembles by Combining Continuous*

Wave and Pulsed EPR Spectroscopy and Molecular Dynamics. Biochemistry, 2010. **49**(10): p. 2140-2149.
70. Stoll, S. and A. Schweiger, *EasySpin, a comprehensive software package for spectral simulation and analysis in EPR.* Journal of Magnetic Resonance, 2006. **178**(1): p. 42-55.
71. Etienne, E., et al., *SimLabel: a graphical user interface to simulate continuous wave EPR spectra from site-directed spin labeling experiments.* Magnetic Resonance in Chemistry, 2017. **55**(8): p. 714-719.
72. Casey, T.M., et al., *Continuous wave W- and D-Band EPR spectroscopy offer "sweet-spots" for characterizing conformational changes and dynamics in intrinsically disordered proteins.* Biochemical and Biophysical Research Communications, 2014. **450**(1): p. 723-728.
73. Molin, Y.N., K.M. Salikhov, and K.I. Zamaraev, *Spin Exchange. Principles and Applications in Chemistry and Biology*. Vol. 8. 1980, New York: Springer-Verlag.
74. Altenbach, C., et al., *Accessibility of nitroxide side chains: Absolute Heisenberg exchange rates from power saturation EPR.* Biophysical Journal, 2005. **89**(3): p. 2103-2112.
75. Chen, M., et al., *Investigation of alpha-synuclein fibril structure by site-directed spin labeling.* Journal of Biological Chemistry, 2007. **282**(34): p. 24970-24979.
76. Der-Sarkissian, A., et al., *Structural organization of alpha-synuclein fibrils studied by site-directed spin labeling.* Journal of Biological Chemistry, 2003. **278**(39): p. 37530-37535.
77. Jao, C.C., et al., *Structure of membrane-bound alpha-synuclein studied by site-directed spin labeling.* Proceedings of the National Academy of Sciences of the United States of America, 2004. **101**(22): p. 8331-8336.
78. Jao, C.C., et al., *Structure of membrane-bound alpha-synuclein from site-directed spin labeling and computational refinement.* Proceedings of the National Academy of Sciences of the United States of America, 2008. **105**(50): p. 19666-19671.
79. Georgieva, E.R., et al., *Membrane-bound alpha-synuclein forms an extended helix: Long-distance pulsed ESR measurements using vesicles, bicelles, and rodlike micelles.* Journal of the American Chemical Society, 2008. **130**(39): p. 12856-+.
80. Soto, C., *Unfolding the role of protein misfolding in neurodegenerative diseases.* Nature Reviews Neuroscience, 2003. **4**(1): p. 49-60.
81. Altenbach, C., et al., *A Collision Gradient-Method to Determine the Immersion Depth of Nitroxides in Lipid Bilayers - Application to Spin-Labeled Mutants of Bacteriorhodopsin.* Proceedings of the National Academy of Sciences of the United States of America, 1994. **91**(5): p. 1667-1671.
82. Klare, J.P. and H.-J. Steinhoff, *Structural Information from Spin-Labelled Membrane-Bound Proteins.* Structure and Bonding, 2014. **152**: p. 205-248.
83. Altenbach, C., et al., *Estimation of inter-residue distances in spin labeled proteins at physiological temperatures: Experimental strategies and practical limitations.* Biochemistry, 2001. **40**(51): p. 15471-15482.
84. Serpell, L.C., et al., *Fiber diffraction of synthetic alpha-synuclein filaments shows amyloid-like cross-beta conformation.* Proceedings of the National Academy of Sciences of the United States of America, 2000. **97**(9): p. 4897-4902.
85. Schweiger, A. and G. Jeschke, *Principles of Pulse Electron Paramagnetic Resonance*. 2001: Oxford University Press.
86. Borbat, P.P. and J.H. Freed, *Pulse Dipolar Electron Spin Resonance: Distance Measurements.* Struct Bond: Structural Information from Spin-Labels and Intrinsic Paramagnetic Centres in the Biosciences, 2014. **152**: p. 1-82.
87. Saxena, S. and J.H. Freed, *Double quantum two-dimensional Fourier transform electron spin resonance: Distance measurements.* Chemical Physics Letters, 1996. **251**(1-2): p. 102-110.

88. Jeschke, G., et al., *Dipolar spectroscopy and spin alignment in electron paramagnetic resonance.* Chemical Physics Letters, 2000. **331**(2-4): p. 243-252.
89. Schoeps, P., et al., *Broadband spin echoes and broadband SIFTER in EPR.* Journal of Magnetic Resonance, 2015. **250**: p. 55-62.
90. Milov, A.D., K.M. Salikhov, and M.D. Shirov, *Application of Eldor in Electron-Spin Echo for Paramagnetic Center Space Distribution in Solids.* Sov. Phys. Solid State (USA), 1981. **23**(4): p. 565.
91. Pannier, M., et al., *Dead-time free measurement of dipole-dipole interactions between electron spins.* Journal of Magnetic Resonance, 2000. **142**(2): p. 331-340.
92. Razzaghi, S., et al., *RIDME Spectroscopy with Gd(III) Centers.* Journal of Physical Chemistry Letters, 2014. **5**(22): p. 3970-3975.
93. Garbuio, L., et al., *Orthogonal Spin Labeling and Gd(III)-Nitroxide Distance Measurements on Bacteriophage T4-Lysozyme.* Journal of Physical Chemistry B, 2013. **117**(11): p. 3145-3153.
94. Yang, Y., et al., *Generic tags for Mn(II) and Gd(III) spin labels for distance measurements in proteins.* Physical Chemistry Chemical Physics, 2017. **19**(39): p. 26944-26956.
95. Bordignon, E. and Y. Polyhach, *EPR Techniques to Probe Insertion and Conformation of Spin-Labeled Proteins in Lipid Bilayers*, in *Lipid-Protein Interactions: Methods and Protocols in Molecular Biology*, J.H. Kleinschmidt, Editor. 2013. p. 329-355.
96. Schmidt, T., et al., *Long Distance Measurements up to 160 angstrom in the GroEL Tetradecamer Using Q-Band DEER EPR Spectroscopy.* Angewandte Chemie-International Edition, 2016. **55**(51): p. 15905-15909.
97. Chiang, Y.W., P.P. Borbat, and J.H. Freed, *The determination of pair distance distributions by pulsed ESR using Tikhonov regularization.* Journal of Magnetic Resonance, 2005. **172**(2): p. 279-295.
98. Tikhonov, A.N., *Solution of Incorrectly Formulated Problems and Regularization Method.* Doklady Akademii Nauk Sssr, 1963. **151**(3): p. 501-&.
99. Jeschke, G., et al., *Direct conversion of EPR dipolar time evolution data to distance distributions.* Journal of Magnetic Resonance, 2002. **155**(1): p. 72-82.
100. Jeschke, G., et al., *Data analysis procedures for pulse ELDOR measurements of broad distance distributions.* Applied Magnetic Resonance, 2004. **26**(1-2): p. 223-244.
101. Srivastava, M. and J.H. Freed, *Singular Value Decomposition Method to Determine Distance Distributions in Pulsed Dipolar Electron Spin Resonance.* Journal of Physical Chemistry Letters, 2017. **8**(22): p. 5648-5655.
102. Srivastava, M., E.R. Georgieva, and J.H. Freed, *A New Wavelet Denoising Method for Experimental Time-Domain Signals: Pulsed Dipolar Electron Spin Resonance.* Journal of Physical Chemistry A, 2017. **121**(12): p. 2452-2465.
103. Worswick, S.G., et al., *Deep neural network processing of DEER data.* Science Advances, 2018. **4**(8).
104. Ibanez, L.F. and G. Jeschke, *General regularization framework for DEER spectroscopy.* Journal of Magnetic Resonance, 2019. **300**: p. 28-40.
105. Jeschke, G., et al., *DeerAnalysis2006 - a comprehensive software package for analyzing pulsed ELDOR data.* Applied Magnetic Resonance, 2006. **30**(3-4): p. 473-498.
106. Edwards, T.H. and S. Stoll, *Bayesian Statistical Methods in the Analysis of DEER Data.* Biophysical Journal, 2016. **110**(3): p. 153a-153a.
107. Srivastava, M. and J.H. Freed, *Singular Value Decomposition Method To Determine Distance Distributions in Pulsed Dipolar Electron Spin Resonance: II. Estimating Uncertainty.* Journal of Physical Chemistry A, 2019. **123**(1): p. 359-370.
108. Jeschke, G., *Validation of Distance Distributions Derived from DEER/PELDOR/DQ-EPR data.* EPR newsletter, 2009. **18**(4).

109. Georgieva, E.R., et al., *Tau Binds to Lipid Membrane Surfaces via Short Amphipathic Helices Located in Its Microtubule-Binding Repeats.* Biophysical Journal, 2014. **107**(6): p. 1441-1452.
110. Hellmich, U.A., et al., *Probing the ATP Hydrolysis Cycle of the ABC Multidrug Transporter LmrA by Pulsed EPR Spectroscopy.* Journal of the American Chemical Society, 2012. **134**(13): p. 5857-5862.
111. Fehr, N., et al., *Early folding events during light harvesting complex II assembly in vitro monitored by pulsed electron paramagnetic resonance.* Biochimica Et Biophysica Acta-Bioenergetics, 2016. **1857**(6): p. 695-704.
112. Theillet, F.X., et al., *Structural disorder of monomeric alpha-synuclein persists in mammalian cells.* European Biophysics Journal with Biophysics Letters, 2017. **46**: p. S396-S396.
113. Polyhach, Y., E. Bordignon, and G. Jeschke, *Rotamer libraries of spin labelled cysteines for protein studies.* Physical Chemistry Chemical Physics, 2011. **13**(6): p. 2356-2366.